Eng. Sci., 2020, 10, 51–57

Engineered Science

DOI: https://dx.doi.org/10.30919/es8d1012

Generation of Continuously Variable-mode Orbital Angular Momentum Beams

Jianchun Xu,[1,4] Lihao Chen,[1] Xiaojun Zhai,[2] Ru Zhang,[1,3] Klaus D. Mcdonald-Maier,[2] Shanguo Huang[1] and Ke Bi[1,4,*]

Abstract

Orbital angular momentum (OAM) beam emitters with compact structure and high performance are highly desirable for wireless communication and radar technology. Here, we propose a compact emitter that only consists of a ring resonator and a feed line. Continuously-variable-mode OAM beams are generated by adjusting the wavelength and transmission path. The basic design principle and specific evaluation index are discussed. Both the simulated and experimental results demonstrate that the proposed emitter obtains the capacity of generating variable-modes. This approach opens a way for designing novel OAM beam emitter with desired properties.

Keywords: antenna, orbital angular momentum, variable mode
Received date: 5 April 2020; Accepted date: 10 May 2020
Article type: Research article

1. Introduction

Angular momentum typically consists of spin angular momentum (SAM) and orbital angular momentum (OAM).[1,2] SAM is associated with the photon spin and circular polarization states, while OAM is dependent on the field of spatial distribution.[3] The OAM beams, which are special electromagnetic waves characterized by helical phase wave front and doughnut-shaped intensity profile,[4] have attracted extensive interests due to their excellent performance in optical imaging, particles manipulating and quantum information processing.[5-9] In addition to these established fields, the OAM beams also have been used in modern optical/microwave communication systems.[10-13] Unlike SAM only having two possible states, the OAM can theoretically provide infinite achievable modes. Owing to the inherent orthogonality among the different modes, the OAM beams have the potential to increase communication capacity and spectral efficiency by encoding information as OAM modes of the beams or using the OAM beams as information carriers for multiplexing.[14,15] Therefore, the OAM beams have attracted considerable attention from both science and engineering.[16]

To enable the practical applications of OAM beams, generating vortex electromagnetic waves is of fundamental importance. Since the helically phased beam was recognized by Allen and co-workers in 1992, substantial devices have been designed for generating OAM beams.[17-21] Common schemes usually use spiral phase plate, spatial light modulator, computer hologram or metasurface to directly modify electromagnetic beams' wave structure for OAM generation.[22-24] The interference between electromagnetic waves also allows vortex beams to be obtained by antenna array. Although many OAM beam generation technologies have been demonstrated in the optical regime, the research of OAM wave in the radio frequency domain is still in its early days.

Spiral phase plate, antenna array, and metasurface can be applied for OAM beams generation in the radio frequency band.[25-28] However, most of the conventional methods have their disadvantages such as complicated structure, difficulties for manufacturing, high cost, and so on, which restricts their practical applications. Especially in the ways of feeding, spiral phase plate and metasurface both need an extra antenna to provide the signal source. This requirement will doubtless increase the size and complexity

[1] *State Key Laboratory of Information Photonics and Optical Communications, School of Science, Beijing University of Posts and Telecommunications, Beijing 100876, China*
[2] *School of Computer Science and Electronic Engineering, University of Essex, Colchester CO4 3SQ, United Kingdom*
[3] *Beijing Key Laboratory of Space-ground Interconnection and Convergence, Beijing University of Posts and Telecommunications, Beijing 100876, China*
[4] *Beijing University of Posts and Telecommunications Research Institute, Shenzhen 518057, China*
* *Corresponding Author*
E-mail: bike@bupt.edu.cn (Ke Bi).

of the whole OAM beam generation system. To date, only a few designs employed single-feed structure to realize OAM beams in the radio frequency domain.[29,30] The typical approaches to generate the OAM beams with a single feed are based on the dielectric resonator or circularly polarized patch antenna.[31] Using these methods, high order transverse magnetic (TM) mode is applied to form the different OAM modes.[32] The design of the three-dimensional helical antenna is also a way to generate OAM beams.[33] Despite the generation of continuously-variable-mode OAM beams, this method relies on the special helical structure and the feed network, and therefore it is not easily integrated. Generally, these designs are not friendly and convenient for the practical applications of OAM beam.

Here, we demonstrate a compact ring-resonator emitter for the generation of continuously-variable-mode OAM beams. It is achieved via the joint phase control of electromagnetic waves propagation path and wavelength variation at diverse frequencies. Compared with the design of metasurface antenna array in our previous work,[21] the continuous phase variation and variable mode is a distinguishing feature of this work. The entire emitter consists of only a ring patch and a feed line. Taking advantage of parameter variation and different operation frequency, the OAM beams with state numbers -1, -2, -3 were respectively generated as examples. More importantly, this scheme shall not be limited at the working frequency presented in this design. Although the application scenario of the proposed design is set in the microwave band, our scheme can be scaled to other bands of the electromagnetic spectrum, offering a blueprint to achieve compact OAM antenna design.

2. Structure and design principle

Fig. 1 shows the schematics of OAM beam emitters with positive and negative states. The radiation layer of the emitter, placed on a 2 mm-thick dielectric layer with a permittivity 2.65, consists of a ring patch and a feed line. It is worthwhile to note that the bottom layer is covered by a metal ground plate with a thickness of 0.018 mm. To satisfy the impedance matching at the desired operating frequency of 10 GHz, the bottom of the feed line needs to be modified. After calculation and optimization, the width d is set to 5.46 mm. Moreover, the patch width c mainly affects the width of resonance peak. A small value means precise phase variation and less interference. However, it is restricted by the requirements of fabricating and signal feeding. After a comprehensive consideration, the value of patch width c is set to 2 mm.

Regarding the size of the ring resonator, the circumference of the ring patch should be an integral number of wavelengths to realize phase control, generating OAM beam with desired mode. The feed signals are input from the bottom of the emitter and oscillate in the ring resonator. Because of the integral multiple of the wavelength, the new incoming signals with the same working frequency will vibrate in resonance with the old signals oscillating in

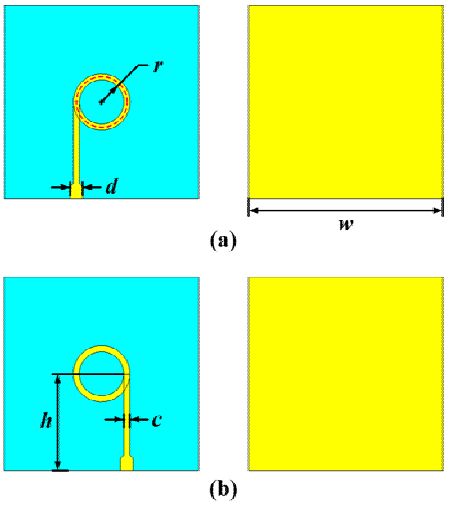

Fig. 1. Schematic diagrams of the ring resonator-based emitters with OAM modes (a) l = 1 and (b) l = -1. Here c is the patch width of the ring resonator, d is the width of the feed line, h is the high of the ring resonator's center, and w is the side length of substrate.

the ring resonator. Meanwhile, the continuous phase variation within an integral multiple of 2π is formed by the transmission of electromagnetic waves in the ring resonator. This phase variation, including a multiple of 2π, is the necessary condition of OAM beam generation. Yet the other signals with different frequencies will arouse weakened oscillation due to the phase difference. Based on the theories described above, the relationship between the wavelength and structure parameter of the ring resonator can be derived and presented as Eq. (1):

$$r = \frac{(l+1)\lambda}{2\pi} \tag{1}$$

where r is the average radius of the ring resonator, l represents the desired mode of generated OAM beam, and λ is the wavelength at operation frequency. For the appropriate size of the whole emitter, the rest of the detailed sizes are designed as w = 56 mm, h = 28 mm. As shown in Fig. 1, the radius r is chosen as 6.46 mm to generate the OAM beams with a mode of l = ±1. The contrary rotation direction of surface current results in positive and negative states generations of OAM beams.

Numerical predictions of the reflection coefficients for the proposed emitter were simulated by using the commercial time-domain package CST Microwave Studio. The boundary condition of 'Open (add space)' is used in all directions and a waveguide port is applied to excite the resonator. All the structure parameters are the same as the above paragraphs. The fabricated emitter, shown in Fig. 2(a), obtains a compact size and simple structure. An SMA connector is welded at the bottom of the fabricated emitter to input feed signal. The simulated and measured reflection coefficients of the proposed emitter with mode l = ±1 are shown in Fig. 2(b). These results both depict approximately the same electromagnetic resonance around 10 GHz. The low reflection coefficients that are less than -20 dB illustrate

well impedance matching. More importantly, the consistency between simulation and measurement demonstrates the rationality of the design.

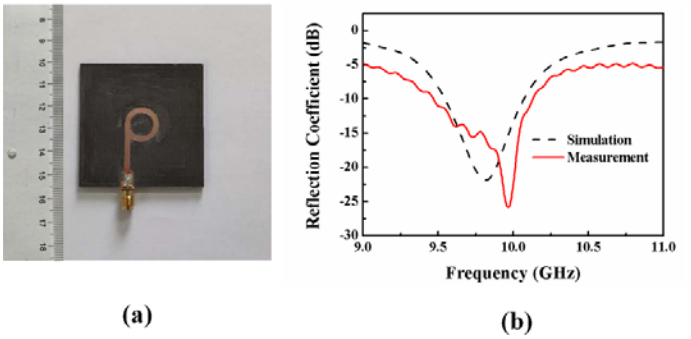

Fig. 2. (a) Photograph of the fabricated OAM beam emitter. (b) Simulated and measured reflection coefficients of the OAM beam emitter with $l = \pm 1$.

3. Results and discussion

In the design of the proposed emitter, the signals resonated in ring resonator and continuous phase variation play an important role in radiation and OAM generation. To understand the principle of the proposed emitter, simulated electric field distributions of phase = 0°, 90°, 180°, and 270° at 9.9 GHz are shown in Fig. 3(a). During one period of the feed signal, the signal in the feed line and the one oscillated in the ring resonator are synchronous, and therefore the junction shows superposition effect. As schematically depicted in Fig. 3(a), the area P has an obvious color. When the signals are weakened by the transmission in the ring resonator, the feed signal can be an unending source to provide energy. The color intensity in the ring resonator and feed line seems nearly, which also demonstrates the superposition effect.

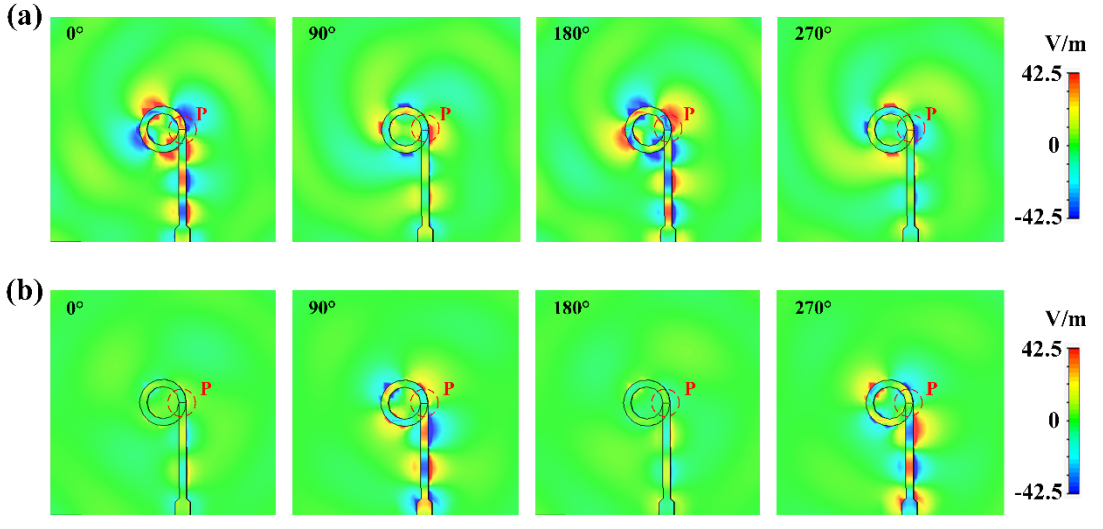

Fig. 3. Simulated electric field distributions of the OAM beam emitter at (a) 9.9 GHz and (b) 8 GHz with a series of phases.

On the contrary, the signal cancellation occurs as a result of the asynchronization between the signals in the feed line and ring resonator. As an example, Fig. 3(b) shows the simulated electric field distributions at the frequency of 8 GHz. From Fig. 3(b), it is observed that the electric field intensity is weak and the connection area P no longer shows superposition effect. This phenomenon indicates that the signals operated at other frequencies cannot be effectively fed and radiated, showing the frequency-selecting property of the proposed emitter.

As mentioned above, appropriate phase control is essential for the OAM beam generation. The size of the ring resonator is modified to achieve different OAM modes. This structure differs from emitter array in having continuous phase variation. Therefore, the shape of helical wave front will be more standard. According to the surface current distribution illustrated in Fig. 4(a), the number of wavelengths in the transmission path (ring resonator) can be easily recognized. The period shown in Fig. 4(a) is 1. Thus, the generated OAM beams obtained the mode of 1.

To provide a theoretical basis for the device fabrication, numerical simulations of the proposed OAM emitter are performed. The setting of the simulations are the same as Fig. 2(b). In addition, the field monitors of electronic field and far field are set up. The simulated results are presented in Fig. 4(b) and 4(c). In the simulations, the observation plane is 300 mm away from the proposed structure with an area of 600 x 600 mm^2. As shown in Fig. 4, one can see the doughnut-shaped intensity profiles and helical phase distributions for generated OAM beams. The mode of the generated OAM beam can be confirmed by the number of the helix and the twist direction. These results demonstrate the generations of OAM beams with the mode of $l = 1$, coinciding well with the above theory and prediction in Fig. 4(a). Here, though only positive state is generated to verify the design, the generations of negative states are distinctly viable employing the above method.

The purity of OAM mode is a significant parameter to

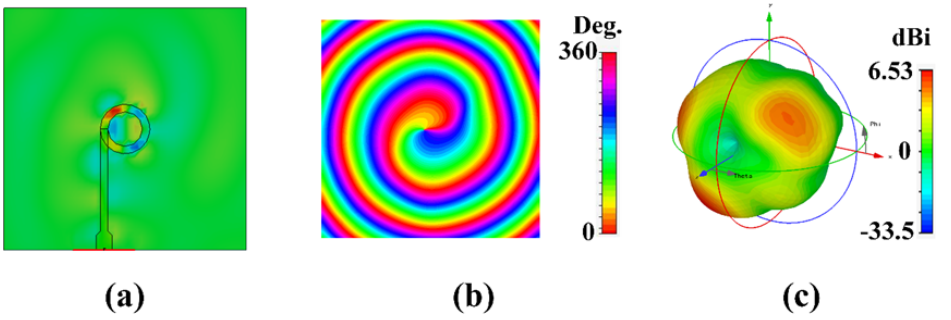

Fig. 4. (a) Surface current distribution of the proposed emitter with OAM mode l = 1. (b) Phase distribution of the generated OAM beam. (c) Radiation pattern of the proposed emitter with l = 1.

evaluate the state of OAM beam. Generally, the generated OAM beams can be regarded as the compound of multiple OAM modes. Based on the principle of Fourier transform, the purity of each mode can be obtained as Eq. (2):[35, 36]

$$p(l) = \frac{1}{2\pi}\int_0^{2\pi} \psi(\phi)\, d\phi \exp(-jl\phi) \tag{2}$$

where l is the mode component of the generated OAM beam, ψ is the phase distribution, ϕ represents the azimuthal angle. Nevertheless, the data is discrete in practical processing. Thus, Eq. (2) can be described as Eq. (3):

$$p[l] = \frac{1}{N}\sum_{n=1}^{N} \psi(\phi_n) \exp(-jl\phi_n) \tag{3}$$

where N is the number of sampling points. Besides, these data points are placed on the circle with max electronic field intensity. As the data is based on the Cartesian coordinate system, the difference values of the data are calculated by the interpolation function. From Eq. (3), the final results are obtained via MATLAB and illustrated in Fig. 5. One can see that, the OAM spectrum weight for OAM mode l = 1 is over 0.9, which means the targeted OAM mode dominates the spectrum. In other words, the proposed emitter performs well in generating desired OAM beams with high mode purity.

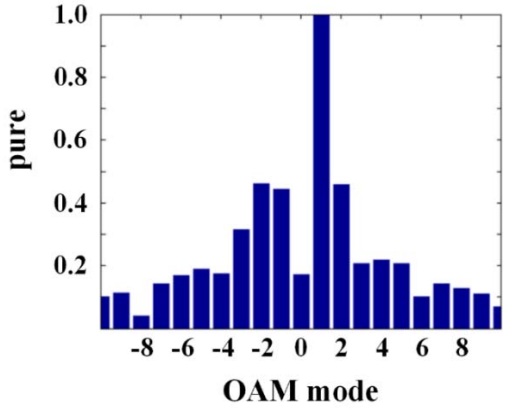

Fig. 5. Histograms of OAM spectrum weight for OAM mode l = 1.

Obviously, only one OAM mode cannot satisfy the requirement of the communication system. But this design provides a method for generating OAM modes with various modes at same operating frequencies. According to the Eq. (1), we note that the average radius r evolves linearly with the mode l of the generated OAM beam while the wavelength is fixed, which indicates that the OAM beams with different modes can be generated by changing the value of r.

In practical application, the structure of the emitter is not easily changed to generate various OAM modes. However, altering the working frequency has no difficulty. From Eq. (1), the relationship between the operating frequency and OAM mode can be obtained and expressed as Eq. (4):

$$f = \frac{(l+1)c}{2\pi rn} \tag{4}$$

where c and n are the light speed in vacuum and refractive index, respectively. With a fixed radius, the mode l becomes linear with the operating frequency. Therefore, the real-time regulation of OAM modes can be realized by altering the working frequency. Based on the established theory, the circumference of the ring resonator also needs to satisfy an integral multiple of wavelength by adjusting the operating frequency, which provides another way to generate various OAM modes.

To verify the practical effect of the proposed emitter in OAM generation, a prototype is fabricated, and a measuring system is designed to measure two-dimensional (2D) near field distribution of generated OAM beam. And the designed measurement system consists of a vector network analyzer (VNA), fabricated emitter, a 2D guide rail, and a horn antenna.

The feed signal came from VNA stimulate the proposed emitter for generating OAM beam through coaxial cable. After a certain space transmission, the near field distribution of the generated OAM beam is received by a horn antenna with the help of a controlled 2D guide rail. In the setting of the measurement system, the guide rail center coincides with the optical axial of generated OAM beam. Limited by the length of the guide rail, the scan range of near field is set as 40×40 cm^2. And the horn antenna is 60 cm far away from the proposed emitter. During the operations, the related information of near field is scanned and recorded layer-by-layer. Then, all measured results are processed and reproduced by MATLAB. The specific

operation is the same as the one employed in Ref.[21].

Fig. 6 depicts the measured 2D received power and phase distribution. One can see that, the doughnut- shaped intensity and spiral phase distribution can be obviously observed, which are the characteristics of OAM beam. Due to the layer-by-layer scan, there are some dislocations in the measured results. The left side of the ring resonator is connected with feed line. Thus, a few distortions in Fig. 6 is generated by the coupling between the ring resonator and feed line. Aperture-coupled technology may improve this problem. The feed line loads on the bottom layer and the ring resonator is then excited through an aperture on the other side of the bottom layer near to the top layer. Here, the resonator is isolated with the feed line. Therefore, the interference between resonator and feed line can be effectively improved.

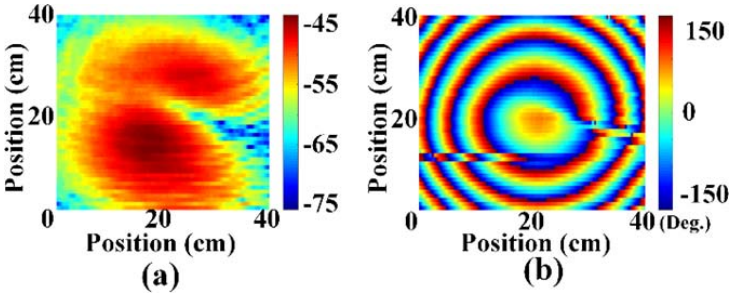

Fig. 6. Measured 2D (a) receive power and (b) phase distribution of OAM mode l = 1.

The above simulations and measurements demonstrate the generation of OAM beam with mode l = 1. Then, we will further discuss the situations of higher modes by a series of simulations. Fig. 7 depicts the electromagnetic response of the proposed emitter with a series of mode l (or r) by using the commercial software CST Microwave Studio. In these simulations, the average radius r is set as 6.46 mm, 9.69 mm, and 12.92 mm to generate the OAM beams with the modes of ±1, ±2, and ±3, respectively. Despite increasing the size of the ring resonator, the OAM beam emitters can have the same operating frequency of 9.9 GHz. This characteristic presents the potential to generate different OAM modes at the same operating frequency. The formula derivation is completed under ideal condition; thus the operating frequency has a few offsets from the initial desired frequency of 10 GHz. A simple and fine adjustment can be provided to solve this problem.

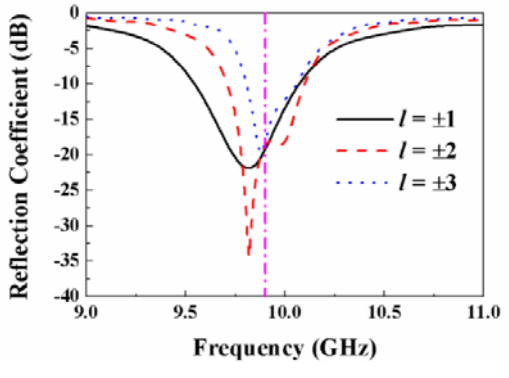

Fig. 7. Simulated reflection coefficients of the OAM beam emitter with a series of modes l.

Employing the above parameters, various models with different OAM modes are simulated. The simulated results are illustrated in Fig. 8. These results also show obvious features of OAM beam, which demonstrates the capacity of the proposed emitter in generating multiple OAM modes. To avoid coincidence in design, negative modes l = -1, -2, -3 were designed and simulated.

After several calculations according to Eq. (4), we can get the theoretical values of operation frequency for various OAM modes (using the above-proposed structure with l = -2 as an example). When the values of OAM mode l are set as 1, 2, and 3, the calculated operation frequencies are around 6 GHz, 9 GHz, and 12 GHz, respectively. In the design of the proposed emitter with l = -2, its reflection coefficients are illustrated in Fig. 9. The determined operation frequencies are 6.7 GHz, 9.9 GHz, and 12.9 GHz, which are nearly coincident with the calculated values. Because of the width of the ring resonator, the resonant peak can't form a pulse-like laser. The surface currents mostly distribute on the edges of the ring resonator, each resonant peak, therefore, has two bulges. This phenomenon is attenuated with a decrease in frequency.

To demonstrate the above theory calculations and predictions of the variable-mode orbital angular momentum beams generations, numerical simulations are performed. The phase distributions and radiation patterns at the frequencies of 6.7 GHz, 9.9 GHz, and 12.9 GHz are shown in Fig. 10. In these simulations, the observed area is increased to 400×400 mm^2 for clear vision. From left to right, the phase distribution exhibits 1, 2, and 3 helixes with clockwise direction and the profiles of the radiations develop 'doughnut' shapes, which indicate the generations of OAM beams with the mode of -1, -2, and -3.

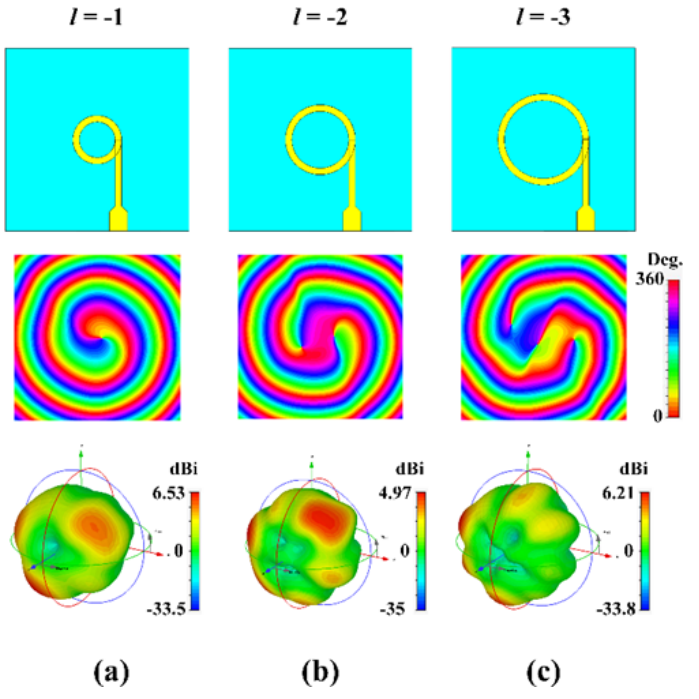

Fig. 8. Structure, phase distributions and radiation patterns for OAM modes of (a) l = -1, (b) l = -2, and (c) l = -3.

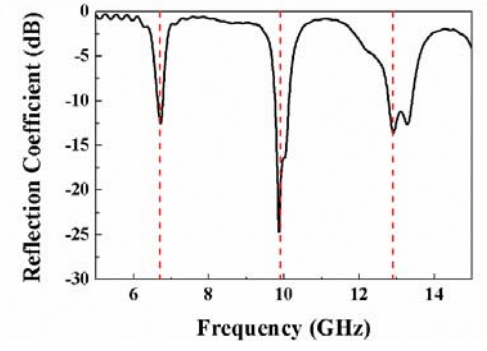

Fig. 9. Simulated reflection coefficient of the OAM beam emitter.

4. Conclusion

Based on the compact ring resonator, we have proposed an effective and simple way to generate OAM beams with various modes in the radio frequency band. The OAM modes are modulated by adjusting the radius of the ring resonator at the same operating frequency or altering the operation frequency. According to the simulated and measured results, the OAM mode of l = 1 is generated to verify the theoretical predictions by employing the above two methods. The standard helical wave front is achieved by the continuous phase control. Utilizing a series of mode analysis and calculations, the high purities of the generated OAM beams are over 0.9. Therefore, we believe this OAM beam emitter, with compact structure and superior performance, has the potential to promote the radio frequency (RF) OAM beams' applications.

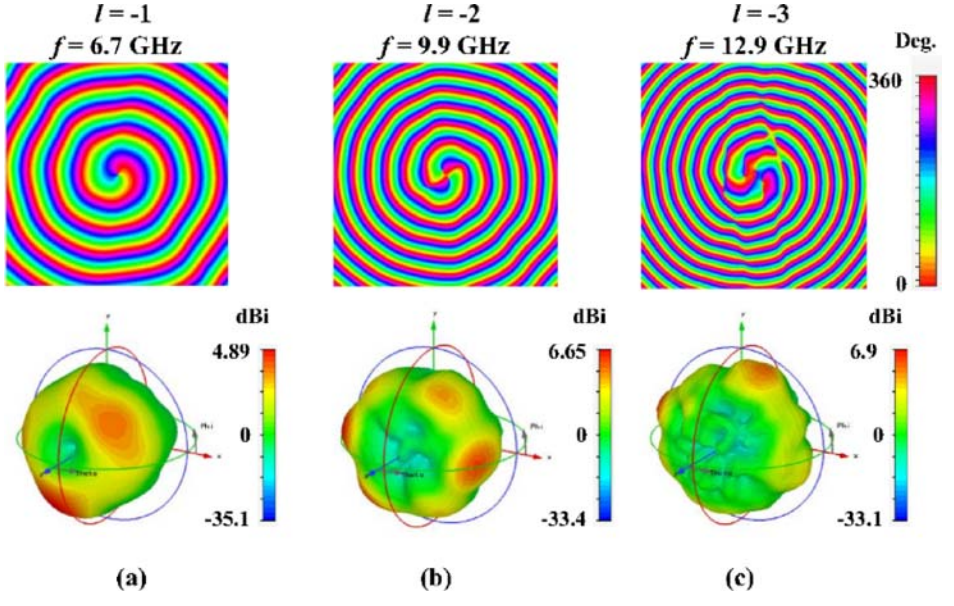

Fig. 10. Simulated phase distributions and radiation patterns at the frequencies of (a) 6.7 GHz, (b) 9.9 GHz, and (c) 12.9 GHz.

Acknowledgements

We are grateful to the anonymous reviewers for their valuable comments and suggestions. Financial supports from the National Natural Science Foundation of China (NSFC) (51972033, 51788104, 61672108, 61976025, and 61675103); Science and Technology Plan of Shenzhen City (JCYJ20180306173235924); Key area research plan of Guangdong (2019B010937001); and Ph.D. student short-term overseas study and exchange program of BUPT are also gratefully acknowledged.

Supporting information

Not applicable

Conflict of interest

There are no conflicts to declare.

References

[1] J. Liu, W. X. Liu, S. T. Li, D. Wei, H. Gao and F. L. Li, *Photonics Res.*, 2017, **5**, 617-622, doi: 10.1364/PRJ.5.000617.

[2] P. Miao, Z. F. Zhang, J. B. Sun, W. Walasik, S. Longhi, N. M. Litchinitser and L. Feng, *Science*, 2016, **353**, 464-467, doi: 10.1126/science.aaf8533.

[3] Y. Yan, G. D. Xie, M. P. J. Lavery, H. Huang, N. Ahmed, C. J. Bao, Y. X. Ren, Y. W. Cao, L. Li and Z. Zhao et al., *Nat. Commun.*, 2014, **5**, 4876, doi: 10.1038/ncomms5876.

[4] J. Q. Zheng, A. Yang, T. Wang, X. L. Zeng, N. Cao, M. Liu, F. F. Pang and T. Y. Wang, *Photonics Res.*, 2018, **6**, 396-402, doi: 10.1364/PRJ.6.000396.

[5] C. Li and S. M. Zhao, *Photonics Res.*, 2017, **5**, 267-270, doi: 10.1364/PRJ.5.000267.

[6] W. X. Qu, Y. Zhang, H. W. Liu, T. Q. Dou, J. P. Wang, Z. H. Li, S. Y. Yang and H. Q. Ma, *J. Opt. Soc. Am. B*, 2019, **36**, 1335-1341, doi: 10.1364/JOSAB.36.001335.

[7] K. Liu, Y. Q. Cheng, Y. Gao, X. Li, Y. L. Qin and H. Q. Wang, *Appl. Phys. Lett.*, 2017, **110**, 164102, doi: 10.1063/1.4981253.

[8] W. X. Qu, H. W. Liu, J. P. Wang and H. Q. Ma, *Opt. Commun.*, 2019, **448**, 43-47, doi: 10.1016/j.optcom.2019.05.003.

[9] X. J. Zhai, M. Eslami, E. S. Hussein, M. S. Filali, S. T. Shalaby, A. Amira, F. Bensaali, S. Dakua, J. Abinahed and A. Al-Ansari et al., *J. Comput. Sci.*, 2018, **27**, 35-45, doi: 10.1016/j.jocs.2018.05. 002.

[10] S. G. Huang, B. L. Guo and Y. A. Liu, *IEEE Commun. Mag.*, 2020, **58**, 13-19, doi: 10.1109/MCOM.001.1900583.

[11] M. Oldoni, F. Spinello, E. Mari, G. Parisi, C. G. Someda, F. Tamburini, F. Romanato, R. A. Ravanelli, P. Coassini and B. Thidé, *IEEE T. Antenn. Propag.*, 2015, **63**, 4582-4587, doi: 10.1109/TAP.2015.2456953.

[12] S. M. Mohammadi, L. K. S. Daldorff, J. E. S. Bergman, R. L. Karlsson, B. Thidé, K. Forozesh, T. D. Carozzi and B. Isham, *IEEE T. Antenn. Propag.*, 2009, **58**, 565-572, doi: 10.1109/TAP.2009. 2037701.

[13] J. Wang, J. Y. Yang, I. M. Fazal, N. Ahmed, Y. Yan, H. Huang, Y. X. Ren, Y. Yue, S. Dolinar and M. Tur et al., *Nat. Photonics*, 2012, **6**, 488-496, doi: 10.1038/nphoton.2012.138.

[14] W. G. Zhu, M. J. Jiang, H. Y. Guan, J. H. Yu, H. H. Lu, J. Zhang and Z. Chen, *Photonics Res.*, 2017, **5**, 684-688, doi:10.1364/PRJ.5. 000684.

[15] A. E. Willner, L. Li, G. D. Xie, Y. X. Ren, H. Huang, Y. Yue, N. Ahmed, M. J. Willner, A. J. Willner and Y. Yan et al., *Photonics Res.*, 2016, **4**, B5-B8, doi: 10.1364/PRJ.4.0000B5.

[16] S. Y. Fu and C. Q. Gao, *Photonics Res.*, 2016, **4**, B1-B4, doi: 10.1364/PRJ.4.0000B1.

[17] J. C. Xu, M. Y. Zhao, R. Zhang, M. Lei, X. L. Gao, S. G. Huang and K. Bi, *IEEE Antenn. Wirel. Pr.*, 2017, **16**, 829-832, doi: 10.1109/LAWP.2016.2606118.

[18] J. Vieira, R. M. G. M. Trines, E. P. Alves, R. A. Fonseca, J. T. Mendonça, R. Bingham, P. Norreys and L. O. Silva, *Nat. Commun.*, 2016, **7**, 10371.

[19] H. X. Xu, H. W. Liu, X. H. Ling, Y. M. Sun and F. Yuan, *IEEE T. Antenn. Propag.*, 2017, **65**, 7378-7382, doi: 10.1109/TAP. 2017. 2761548.

[20] N. Zhou, S. Zheng, X. P. Cao, Y. F. Zhao, S. Q. Gao, Y. T. Zhu, M. B. He, X. L. Cai and J. Wang, *Sci. Adv.*, 2019, **5**, eaau9593, doi: 10.1126/sciadv.aau9593.

[21] J. C. Xu, Y. N. Hao, K. Bi, R. Zhang, S. G. Huang and J. Zhou, *Eng. Sci.*, 2019, **6**, 30-35, doi: 10.30919/es8d748.

[22] E. Maguid, I. Yulevich, D. Veksler, V. Kleiner, M. L. Brongersma and E. Hasman, *Science*, 2016, **352**, 1202-1206, doi: 10.1126/science.aaf3417.

[23] G. M. Vanacore, G. Berruto, I. Madan, E. Pomarico, P. Biagioni, R. J. Lamb, D. McGrouther, O. Reinhardt, I. Kaminer and B. Barwick et al., *Nat. Mater.*, 2019, **18**, 573-579, doi: 10.1038/s41563-019-0336-1.

[24] T. Lei, M. Zhang, Y. R. Li, P. Jia, G. N. Liu, X. G. Xu, Z. H. Li, C. J. Min, J. Lin and C. Y. Yu et al., *Light Sci. Appl.*, 2015, **4**, e257, doi: 10.1038/lsa.2015.30.

[25] X. L. Ma, M. B. Pu, X. Li, C. Huang, Y. Q. Wang, W. B. Pan, B. Zhao, J. H. Cui, C. T. Wang and Z. Y. Zhao et al., *Sci. Rep.*, 2015, **5**, 10365, doi: 10.1038/srep10365.

[26] T. Arikawa, S. Morimoto and K. Tanaka, *Opt. Express*, 2017, **25**, 13728-13735, doi: 10.1364/OE.25.013728.

[27] C. M. Liu, J. S. Liu, L. Niu, X. L. Wei, K. J. Wang and Z. G. Yang, *Sci. Rep.*, 2017, **7**, 3891, doi: 10.1038/s41598-017-04373-6.

[28] H. Zhao, B. G. Quan, X. K. Wang, C. Z. Gu, J. J. Li and Y. Zhang, *ACS Photonics*, 2018, **5**, 1726-1732, doi: 10.1021/acsphotonics. 7b01149.

[29] W. T. Zhang, S. L. Zheng, X. N. Hui, Y. L. Chen, X. F. Jin, H. Chi and X. M. Zhang, *IEEE Antenn. Wirel. Pr.*, 2017, **16**, 194-197, doi: 10.1109/LAWP.2016.2569540.

[30] H. Su, X. P. Shen, G. X. Su, L. Li, J. P. Ding, F. X. Liu, P. Zhan, Y. M. Liu and Z. L. Wang, *Laser Photonics Rev.*, 2018, **12**, 1800010, doi: 10.1002/lpor.201800010.

[31] M. Barbuto, F. Trotta, F. Bilotti and A. Toscano, *Prog. Electromagn. Res.*, 2014, **148**, 23-30, doi: 10.2528/PIER14050204.

[32] J. J. Liang and S. L. Zhang, *IEEE Access*, 2016, **4**, 9570-9574, doi: 10.1109/ACCESS.2016.2636166.

[33] F. Shen, J. N. Mu, K. Guo, S. M. Wang and Z. Y. Guo, *IEEE Antenn. Wirel. Pr.*, 2019, **18**, 1091-1095, doi: 10.1109/LAWP.2019. 2907931.

[34] L. L. Wang, H. Y. Chen, K. Guo, F. Shen and Z. Y. Guo, *Electronics*, 2019, **8**, 251, doi: 10.3390/electronics8020251.

[35] R. Zambrini and S. M. Barnett, *Phys. Rev. Lett.*, 2006, **96**, 113901, doi: 10.1103/PhysRevLett.96.113901.

[36] E. Yao, S. Franke-Arnold, J. Courtial, S. Barnett and M. Padgett, *Opt. Express*, 2006, **14**, 9071-9076, doi: 10.1364/OE.14.009071.